Asymmetry of strain rate sensitivity between up-and down-changes in 6000 series Aluminium alloys of varying Si content

M.R. R Langille, B. J. Diak, Frédéric de Geuser, A. Deschamps, G. Guiglionda

Asymmetry of strain rate sensitivity between up- and down-changes in 6000 series Aluminium alloys of varying Si content

*M. R. Langille[1,2], B. J. Diak[3], F. De Geuser[2], A. Deschamps[2], G. Guiglionda[1]

[1] *Constellium Technology Center (C-TEC)*
Voreppe, France

[2] *Univ. Grenoble Alpes, CNRS, Grenoble INP, SIMaP*
F-38000 Grenoble, France

[3] *Mechanical and Materials Engineering, Queen's University*
Kingston, ON, Canada

*(*Corresponding author : michael.langille@constellium.com)*

Abstract

Increasing demand for a reduction in fuel emissions in passenger vehicles has generated the need for lighter weight materials to be used in automobile manufacture for body-in-white applications. Aluminium alloys in the 6000-series, containing Mg and Si are ideal candidates for these applications but lack the formability found in commonly used steels, providing a need to more fully understand the factors influencing the formability of these alloys at high strains. Conventionally, a high strain rate sensitivity (SRS) is tied to increased formability because it retards the increase in the local strain rate found in the diffuse neck interior. However, most experimental work neglects that the regions exterior to the neck will undergo a local decrease in the strain rate which causes a corresponding material softening. Observations of an asymmetry between up-change and down-change SRS of these alloys in the natural aged condition show that different mechanisms are controlling the SRS depending on the direction of rate change. Following a characterization of the state of clustering by differential scanning calorimetry, continuous tensile and precision strain rate sensitivity testing results are presented, elucidating the differences between the up-change and down-change SRS tests. It is shown that these differences are due to the activation of different thermal obstacles during the two directions of rate changes. The role of a change in Si content on the mechanical properties is explored and its suspected role on the asymmetric SRS is discussed.

Keywords: natural ageing, necking, recovery, strain rate sensitivity, strain hardening; Al-Mg-Si

1.0 Introduction

The use of aluminium alloy sheet metal in the automotive industry for body-in-white applications has established the requirement for a better understanding of the deformation behaviour and high-strain mechanical properties of these alloys. The production of automobile doors, roofs, and hoods, all introduce plastic strain to the sheet metal with industrial designers constantly pushing the limits of the material properties to produce the most desirable vehicles while manufacturers are attempting to reduce the mass of passenger vehicles to meet environmental standards [1], [2]. The result is that automotive manufacturers desire aluminium alloy sheets with increased formability to allow more complex designs to be created using thinner sheet metal without failure. In forming practices, once a sheet has developed a localized neck, it is considered to be in a failed state and the part is rejected.

The transition from diffuse to localized necking is not fully understood but conventionally, the Considère criterion [3] is employed to determine the onset of diffuse necking. It relates the current strain hardening, $d\sigma/d\epsilon$, to the current flow stress, σ, whereby once $d\sigma/d\epsilon = \sigma$ is met, a geometric instability develops resulting in flow localization [4]–[6]. This flow localization yields an increased strain rate within the neck interior. It has been shown that materials with a large strain rate sensitivity (SRS) at high strains near the Considère criterion will delay the onset of localized necking [4], [6]–[10]. This effect is attributed to the local increase in the strain rate upon diffuse necking, which changes the local flow stress and strain hardening states. Conversely, little attention has been given to the region outside of the neck whereby the local strain rate will inevitably decrease [7] in order to maintain the overall imposed deformation rate.

The strain rate sensitivity of the flow stress is an important parameter for understanding the necking behaviour but its determination requires significant care. Strain rate sensitivity has historically being measured by tensile testing multiple specimens at various strain rates [11], [12], stress relaxation, or by strain rate change or jump tests of single specimens [13]–[17]. Of the three approaches, only the strain rate change test can extract a model independent activation volume, V [14]. When performing strain rate change tests, the machine and specimen stiffness result in an elastic response to the newly imposed strain rate, and an associated stress change, which can lead to experimental errors. This effect is magnified if a decrease in the strain rate is applied or if the change in the strain rate is significantly large [18], [19]. Consequently, reliable instantaneous strain rate sensitivity values to determine thermodynamic parameters are elusive for most laboratories with most measurements being reported from tests that increase the strain rate (where the system naturally stiffens).

When reliable strain rate sensitivity measurements are made by either increasing or decreasing strain rates, an asymmetry of the SRS for dilute alloys has been observed at high strains (high flow stresses) [13], [20], [21], namely the sensitivity to a decrease in strain rate is found to be greater than that of an increase at room temperature. During necking, such an asymmetry results in a difference between the relative increase and decrease of flow stress within the neck interior and exterior, respectively: the magnitude of the stress decrease in the neck exterior is greater than the relative stress increase in the neck interior, which may be hypothesized to reduce the localization of plastic flow.

Since the strain rate sensitivity of aluminium and aluminium alloys has been perceived in the general literature to be negligible compared to materials like steels, there has been no effort to consider how alloying and microstructural design might contribute to this asymmetry to enhance neck prevention in sheets. Design of 6000-series aluminium alloys for automotive sheets has been a very active research area over the last 10 years, with much focus on optimizing the paint bake hardening response, i.e. the strength increase that happens due to precipitation during the paint bake heat treatment, consisting of ~20 min at ~185 °C. It is now well established that in 6000-series alloys, the paint bake hardening response strongly depends on alloy composition and on the presence of clusters, whose characteristics depend on the heat treatment (time of natural ageing, pre-ageing treatment) [22]–[25]. Conversely, the influence of alloy composition and

the presence of clusters on the strain hardening behaviour and on the SRS has been the object of very little research [26], despite the necessity to optimize globally the formability of the alloys and their end mechanical properties.

The aim of the present paper is to precisely measure the strain rate sensitivity of the flow stress for different 6000-series Al alloys containing variable amounts of Si, and thus determine the role of Si content on the asymmetry of the rate sensitivity. The paper starts with a brief review of the theory of thermally active flow in order to present the important measureable parameters before describing the experimental details.

2.0 Background

Strain rate sensitivity experiments are used to determine the reversible component of deformation during plastic flow, that is, the portion of activation energy dislocations carry as they overcome obstacles within the material [14], [27]–[29]. In the initial variable temperature experiments by Cottrell and Stokes [30], the components of thermal energy available to the system were adjusted by temperature changes and the resulting changes in stress were measured. Since then, experimentally easier tests have been employed whereby the current strain rate is adjusted by a factor and the resulting change in the applied stress is measured. The basis of SRS is derived from the rate equation for plasticity such that

$$\dot{\epsilon} = \dot{\epsilon_0} \exp\left(-\frac{\Delta G(\sigma)}{kT}\right) \quad (1)$$

where $\dot{\epsilon}$ is the applied plastic strain rate, $\dot{\epsilon_0}$ the base strain rate, $\Delta G(\sigma)$ is the stress-dependent activation energy barrier, k is the Boltzmann constant and T the absolute temperature. For an instantaneous change in strain rate, Eq. 1 is partially differentiated with respect to σ at constant structure, Σ, and temperature, T, such that

$$\left.\frac{\partial \ln \dot{\epsilon}}{\partial \sigma}\right|_{\Sigma,T} = \left.\frac{\partial \ln \dot{\epsilon_0}}{\partial \sigma}\right|_{\Sigma,T} - \left.\frac{1}{kT}\frac{\partial \Delta G(\sigma)}{\partial \sigma}\right|_{\Sigma,T} \quad (2)$$

Assuming $\partial \ln \dot{\epsilon}_0 / \partial \sigma$, is zero, it is possible to define the inverse apparent activation volume 1/V' from equation (2) as

$$\frac{1}{V'} = \left.\frac{1}{kT}\frac{\partial \sigma}{\partial \ln \dot{\epsilon}}\right|_{T,\Sigma} \quad (3)$$

so that $1/V' = -\partial\sigma/\partial \Delta G(\sigma)$. As the equation is initially derived using the shear stress, $\tau = \sigma/M$, and shear strain, $\gamma = M\epsilon$, are used in all calculations, where M is the Taylor factor of 3 used in this work. The apparent activation volume is directly related to the spacing between the rate controlling obstacles, l, the activation distance, d, and the Burgers vector, b, as $V' = bdl$ [31]. An increase in the strain rate is analogous to a decrease of the test temperature performed by Cottrell and Stokes, thus probing the obstacles that control the plastic flow at lower temperature, whereas a decrease in the strain rate probes the rate-controlling obstacles equivalent to testing at a relatively higher temperatures [32], [33]. The evolution of V' during deformation, and thus with increasing flow stress due to strain hardening, is the method to determine the thermodynamic strain rate sensitivity, S, which may be calculated as

$$S = \frac{1}{T}\frac{\partial \sigma}{\sigma\, \partial \ln \dot{\epsilon}} = \frac{1}{T}\frac{\partial \ln \sigma}{\partial \ln \dot{\epsilon}} = \frac{1}{T}\frac{\Delta \ln \sigma}{\Delta \ln \dot{\epsilon}} \quad (4)$$

where the Δ replaces ∂ in the experimental representation. Measuring and plotting $(1/T)\, \Delta\sigma / \Delta \ln \dot{\epsilon} = k/V'$ versus the true stress, σ, yields the Haasen plot [34]. For simplicity, Haasen plots and analyses will be constructed using the change in the flow stress, $(1/T)\, \Delta\sigma/\Delta\, ln\, \dot{\epsilon}$ versus the reduced flow stress, $\sigma - \sigma_{0.2\%}$, to account for the grown-in obstacles from the heat treatments. In the case of fully-recrystallized, pure aluminium, the Haasen plot intersects the plot origin and evolves linearly until failure as the rate controlling obstacles are forest dislocations where $1/V' \propto \sqrt{\rho} \propto (\sigma - \sigma_{0.2\%})$ [14], [30], [34]. However, in age-hardenable alloys, the intercept and initial slope of the Haasen plot are expected to be different from pure aluminium due to the presence of obstacles other than forest dislocations such as solute atoms, clusters, and precipitates. In such materials, as strain hardening progresses and the dislocation density rapidly increases, a change in density of rate-controlling obstacles and thus in activation volume occurs. If one assumes a linear summation of the relative contributions of different obstacles to strengthening [35], [36], [37], then the linearity of the Haasen plot is preserved:

$$\sigma = \sigma_0 + \sigma_1 + \sigma_2 \quad (5)$$

where σ_0 is the intrinsic strength of the material, σ_1 is the contribution due to the presence of clusters or precipitates (assumed to be constant with $\sigma_0 + \sigma_1 = \sigma_{0.2\%}$) and σ_2 is the contribution due to dislocations generated by subsequent deformation. This representation can then be extended and substituted into Eq. 4 for σ and then used to determine the total thermodynamic strain rate sensitivity as $S = S_1 + S_2$.

3.0 Experimental Details

Three aluminium alloys were tested having a nominal composition of Al-0.35Mg-0.2Cu (wt%) with 0.9, 1.1 or 1.3 wt% Si. The samples were received in the as-rolled condition, solution heat treated in an air furnace at 550°C for 15 minutes, water-quenched (to 15°C) and allowed to naturally age for one month. Specimens from each alloy were tested using a Mettler Toledo differential scanning calorimeter (DSC) at a heating rate of 20°C /min up to 300°C in both the water quenched (WQ) and 1 month NA conditions (NA1m). Tensile tests were performed using a servo-hydraulic Instron 8502 with a 5 kN load cell and a dynamic 25 ± 10 mm extensometer. Tensile dog-bone specimens were machined from 1 mm thick sheet with a gauge length of 30 mm and a width of 10 mm in the rolling direction. The samples were pulled at 294 K (23°C) and a true strain rate of 5×10^{-4} s^{-1} until failure to determine the true stress versus true plastic strain tensile curves and corresponding strain hardening evolution.

Strain rate sensitivity tests were performed using the same base strain rate and strain rate change factors of 4, or 1/4 and 1/10, for the up-change and down-change rate changes, respectively. A proprietary software controlling a feedback-loop to the initial and active extensometer displacement was used to control the true strain rate and strain rate change allowing for precise measurement of the strain rate sensitivity [18]. In order to correctly perform the strain rate change tests, the step-ramp method originally implemented by Carlone and Saimoto [18] for servo-hydraulic systems was used whereby a "step" is inserted during the rate change in order to dynamically compensate for the difference in machine and specimen stiffness at the two different strain rates. The step changes based on the strength of the sample, the extent of strain hardening, the stiffness of the testing machine, and depends on both the direction of the strain rate change (up or down) as well as the change factor (4, 10, 1/4, 1/10, etc). For the machine used in this work, compensation steps of 0.5 to 10 µm were used in down-changes. The step-ramp compensation is naturally less for increasing strain rate change tests in tension due to the inherent increase in machine stiffness such that steps of 0.05 – 1 µm were used for up-changes.

4.0 Results and Analysis

4.1 Microstructure and constant strain rate properties

Figures 1a and 1b show DSC thermograms for the three alloys respectively in the water quenched and naturally aged states, which give indications on the state of clustering in the conditions prior to tensile testing. In the water quenched condition, the thermogram shows a first exothermic peak centered around 100°C, followed by an endothermic peak around 220°C and a sharp exothermic peak around 250°C. Based on the literature [38], [39], the first peak can be identified as the formation of clusters during the DSC heating ramp, the second to the partial dissolution of these clusters, and the third to the formation of hardening precipitates such as β''. From the results of Figure 1a, an addition of Si increases the formation of clusters and enhances the formation of β''. It can be expected that the increased formation of clusters happening during continuous heating also occurs during room temperature natural ageing, so that in a naturally aged condition the higher-Si content alloys contain a larger amount of clusters than lower-Si content alloys.

In the NA1m condition (Figure 1b), the first exothermic peak has disappeared, which can be related to the initial presence of clusters formed during natural ageing. These clusters are observed to dissolve progressively over a wide temperature range, starting at 50°C and extending to the temperature where precipitation starts. This dissolution peak could be the convolution of the dissolution of two types of clusters (such as Si-rich

and Mg-rich) as has been proposed in the literature [40]–[44]. Although the addition of Si results in a larger quantity of clusters, their dissolution peak in Figure 1b is globally of lower magnitude, meaning that Si decreases their thermal stability. However, in a description by two types of clusters for this dissolution behaviour, the data suggests that the magnitude of the low-temperature dissolution peak (120-140°C) is increased by the addition of Si whereas the contrary applies to the high-temperature peak (~240°C) suggesting that Si additions increase the proportion of the lower thermal stability cluster species formed during NA. Additionally, the precipitation starting temperature of the naturally aged materials is strongly shifted to higher temperatures as compared to the as-quenched condition, illustrating the well-documented negative effect of natural ageing on paint-bake hardening response [45]–[47]. This negative effect is of lower magnitude in the high Si alloy which shows in the naturally aged condition a lower precipitation temperature as compared to the other alloys.

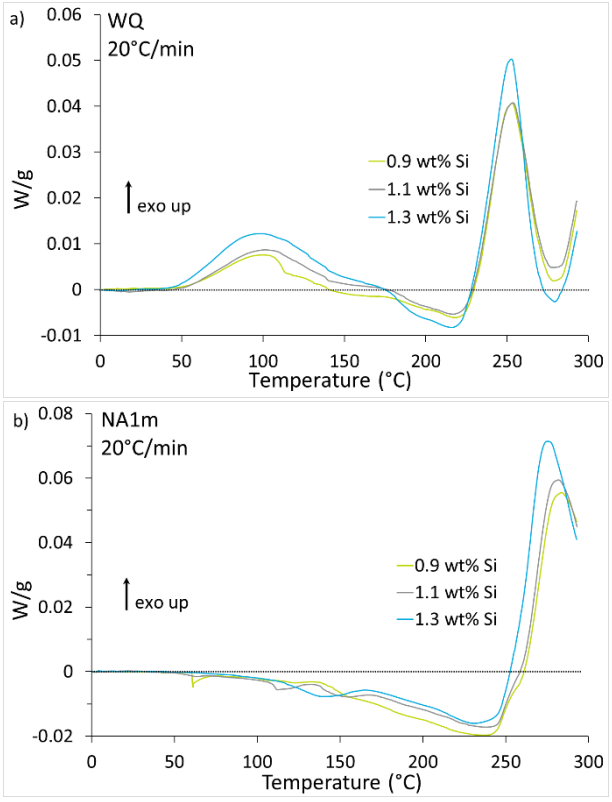

Figure 1: *DSC scans for the three alloys studied after solutionizing at 550°C for 15 minutes, WQ and after* ***a)*** *zero NA, and* ***b)*** *NA1m. The exothermic (exo up) direction for clustering or precipitation is positive.*

Figure 2a presents the true stress-true plastic strain curves and Figure 2b the corresponding strain hardening behaviour in a Kocks-Mecking representation of the stain hardening rate versus the stress increment after yielding for the three alloys tested in the naturally aged condition. The addition of Si increases the yield strength, tensile strength, and instantaneous strain hardening rate throughout the tensile test. As a consequence, despite a higher yield strength, the addition of Si results in an increased uniform elongation via an increase in the strain hardening capacity. The strength increase with Si addition is consistent with the higher amount of clustering observed during DSC experiments. All stress-strain responses displayed stable flow during straining.

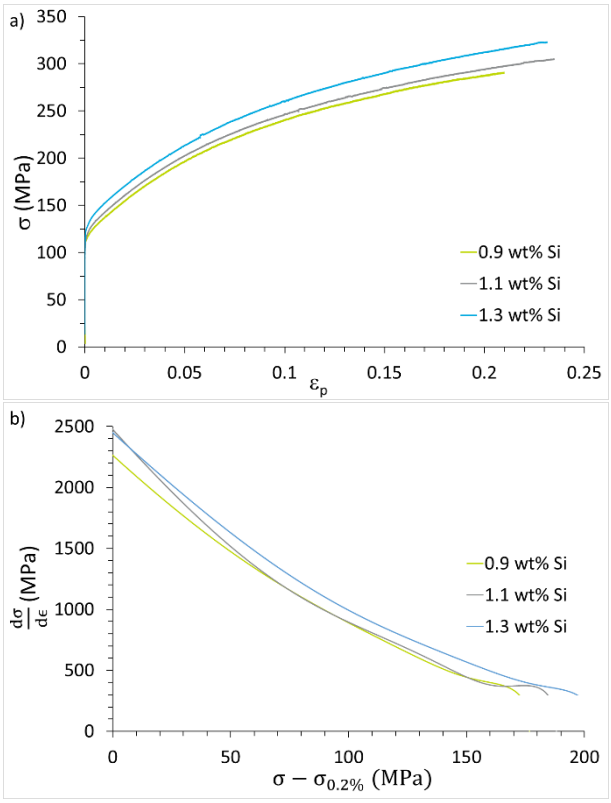

Figure 2: *The effects of Si additions after water quenching followed by NA for 1 month. Samples were tested at 294K at a constant true strain rate of 5 x 10^{-4} s^{-1}.* ***a)*** *True stress versus true plastic strain and* ***b)*** *Kocks-Mecking plot showing the evolution of strain hardening.*

4.2 Strain rate sensitivity testing method

The importance of the step-ramp method is shown below in Figures 3a and 3b, the strain and stress evolution over time is shown for a strain rate down

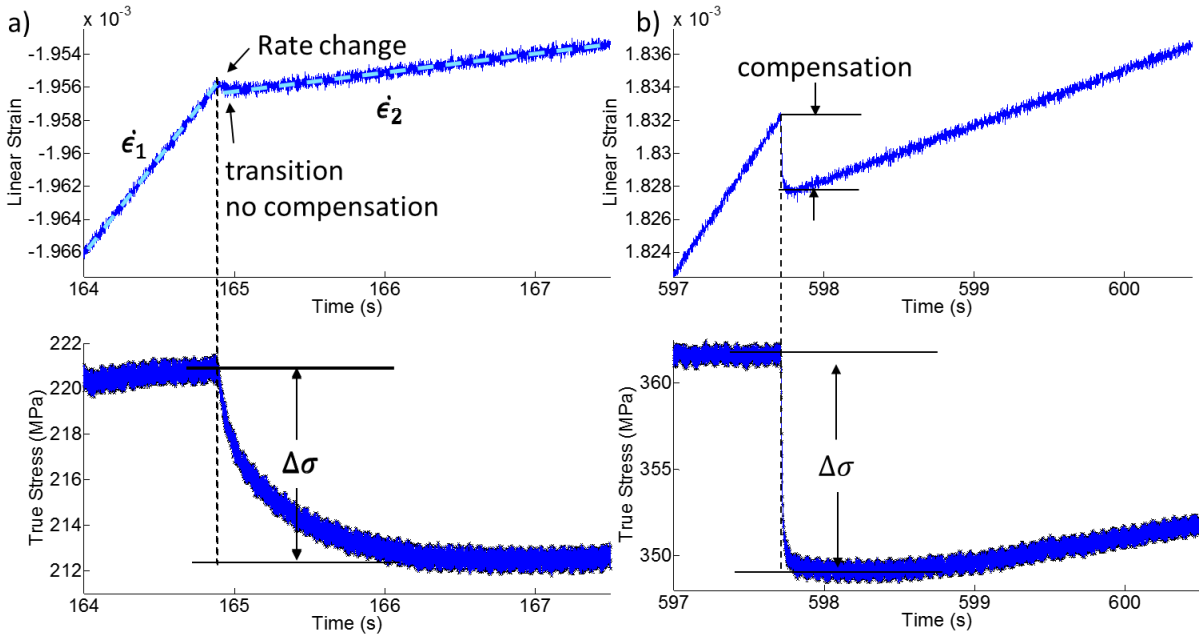

Figure 3: *The time dependence of the true strain control and true stress response with a strain rate change for an Al-0.35Mg-1.3Si-0.5Cu test sample with* ***a)*** *no compensation (traditional method), and* ***b)*** *ideal compensation. Note the stress relaxation over longer time to reach a minimum stress in the un-compensated test compared to the compensated one.*

change test without (Figure 3a) and with (Figure 3b) a step introduced during the rate change.

When observing the evolution of both strain and stress over time, it is clear that elastically compensating the system to match the plastic strain rate change substantially reduces the time taken to reach the minimum stress. Without compensation (Figure 3a), the sample relaxes due to the elastic unloading of the machine and sample and a stress minimum is observed after several seconds compared to sub-second for the compensated tests. The result is that the total stress change is lower, and the apparent activation volume will be artificially higher than characteristic of the rate controlling obstacle (reducing its level on the Haasen plot and leading to a smaller apparent SRS). Without compensation, ad hoc back-extrapolation methods have been used in the literature to estimate an "instantaneous" stress drop from after these relaxations [17], [48], [49].

Figures 4a and 4b shows the evolution of strain and true stress with time along an up-change of strain rate with a very small step ramp. Two different stress changes can be identified corresponding to the instantaneous stress change measured at the peak stress, and the transient stress change corresponding to a stress plateau at much later times. Although both stresses have been used in the literature [15], [21], [33], we will use the instantaneous stress change throughout the paper as it is more relevant to the understanding of non-constant strain rate processes such as necking. The two strain rate regions are denoted in Figure 4a and the measured stress increase is indicated in Figure 4b.

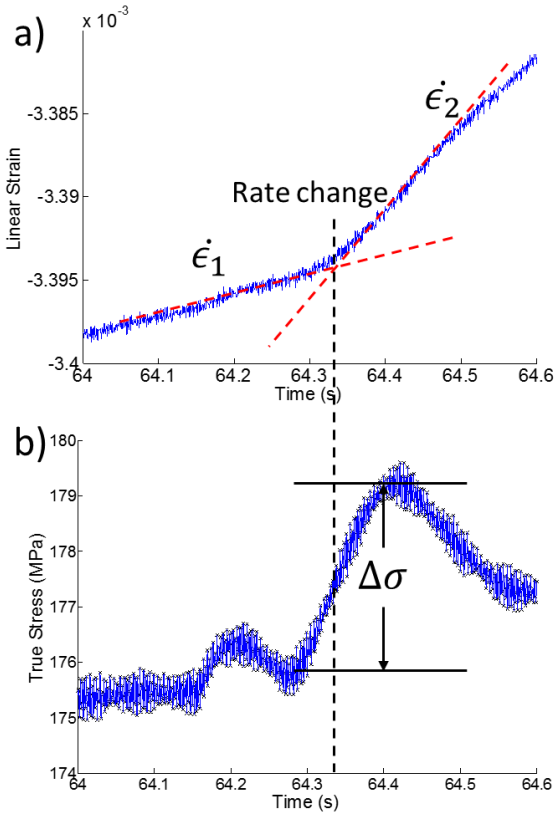

Figure 4: *Method used to determine the up-change response of strain-jump tests. The vertical line delineates the transition between the* ***a)*** *initial and the increased strain rate over time. The difference of the* ***b)*** *stress over time is between the region still within the first strain rate and the region where the increased strain rate is now active. The initial fluctuation in the stress before the rate change at 64.2 s is due to the start of a strain control segment just before the new rate and step are applied.*

4.3 Strain rate sensitivity results

Tensile tests with intermittent strain rate changes by a factor of 4, 1/4, and 1/10 were carried out on the three alloys in the NA1m condition. The Haasen plots constructed from the measured stress changes are shown in Figures 5a-c. The key parameters for each of the curves on the Haasen plot were determined as follows. The different regions and directions of strain rate changes were fit piece-wise. The S_4 curve (up-change x4) was fit using a single straight line for the entire test, despite the flattening out that is observed in these tests at the highest stresses. The $S_{1/10}$ and $S_{1/4}$ (respectively 1/10 and 1/4 down changes) slopes were taken at the point of deviation from the initial S_4 slope, starting at ~40 MPa of strain hardening until linear regression failed. $S_{1/10}$, namely the Haasen plot slope for the 1/10 down changes, is slightly but significantly larger than $S_{1/4}$. In the following, the combined 1/4 and 1/10 tests were used to determine an average intercept (used in further calculations). This was required due to the fact there is no asymmetry between up and down changes in the Haasen plot value, i.e. in the inverse activation volume, directly after yield and in the early stages of strain hardening. In theory, as will be subsequently discussed, the onset of the asymmetry should be independent of the strain rate change amplitude and the Haasen plot slope is the relevant parameter. In order to visualize the effect of Si addition on the strain rate sensitivity, the data of the three alloys are plotted together in Figure 6.

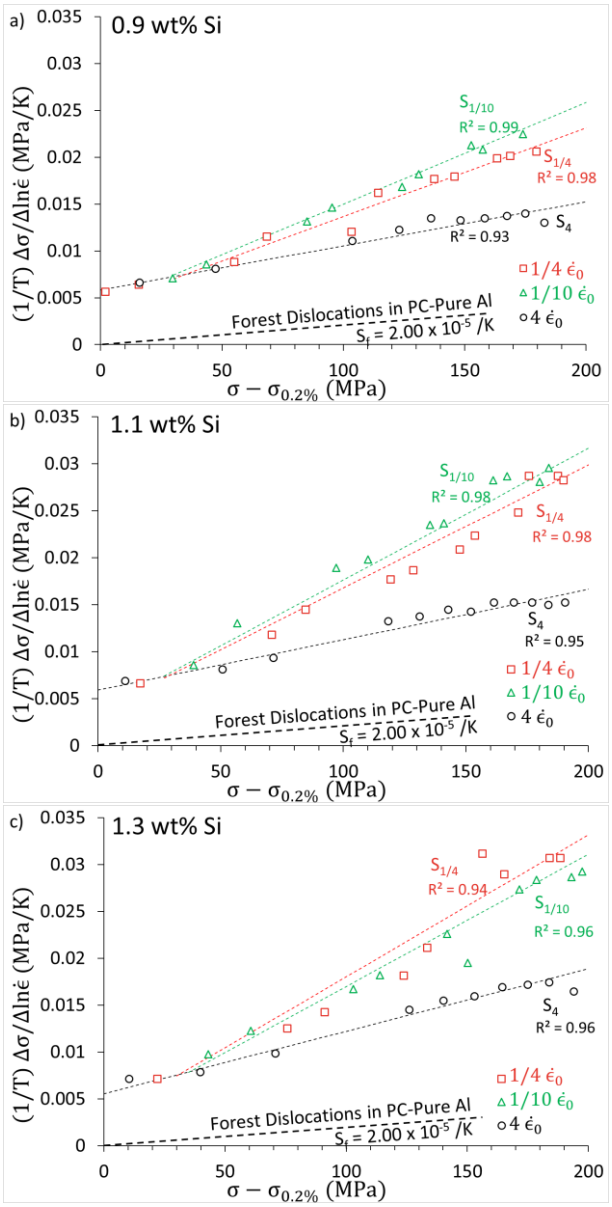

Figure 5: *The Haasen plots constructed using the compensation methods for the* ***a)*** *0.9 wt% Si,* ***b)*** *1.1 wt% Si, and* ***c)*** *1.3 wt% Si. The samples were tested at a base strain rate of 5 x 10^{-4} s^{-1} and a test temperature of 294 K. Note the large differences between the down-change and up-change tests at higher work-hardened*

states. The use of ¼ (open red squares) and 1/10 (open green triangles) strain rate changes were applied for the down-change tests, while a change factor of 4x (open black circles) was used for the up-change tests. Also shown is the behaviour for high purity polycrystalline aluminium at the same temperature.

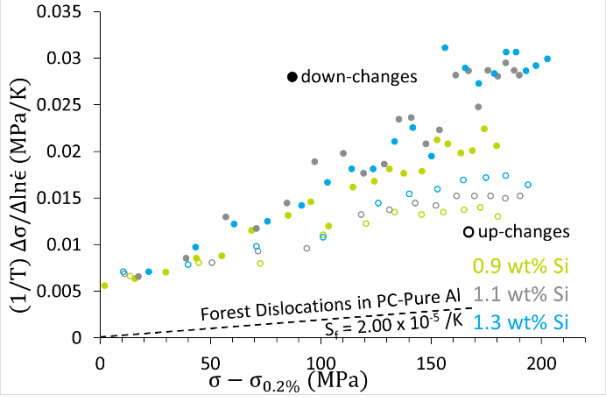

Figure 6: *The Haasen plot illustrating the effects of Si on the evolution of the inverse activation volume during strain hardening. The 1/4 and 1/10 down-changes (closed symbols) are not identified separately in this plot. It is clear that the inverse activation volume from yield to about 40 MPa is similar for all alloys independent of the direction of the rate-change.*

Several trends can be observed in the Haasen plot and specifically the evolution of $(1/T)\ \Delta\sigma/\Delta\ ln\ \dot{\epsilon} = k/V'$ with stress, where V' is the apparent activation volume. Initially, k/V' for all alloys whether probed by up or down rate changes is similar at yield and follows a Cottrell-Stokes behaviour for the first 40 MPa of hardening similar to the pure Al dislocation-dislocation line (dashed line), which can be correlated to the first 0.04 strain in the Kocks-Mecking plot of Figure 2b. The positive intercept on the Haasen plot indicates an obstacle contribution to the flow stress that is more rate sensitive than dislocations. This behaviour continues with the up-change measurements to higher stresses, but increases more rapidly with the down-rate changes: the 1/4 stress changes have a lower Haasen slope compared to the 1/10 stress changes for low 0.9 and 1.1 wt% Si alloys. The addition of Si increases k/V' at high strains for both the up-change and down-change tests compared to the 0.9 wt% Si base alloy. Since the initial values of k/V' are similar for all three alloys, this variation at large strains results in a slope change of the Haasen plot, i.e. in a larger thermodynamic strain rate sensitivity, S, for increasing Si content. The S values determined from testing the three alloys with different strain rate changes are summarized in Figure 7, based on the fits in Figures 5a-c.

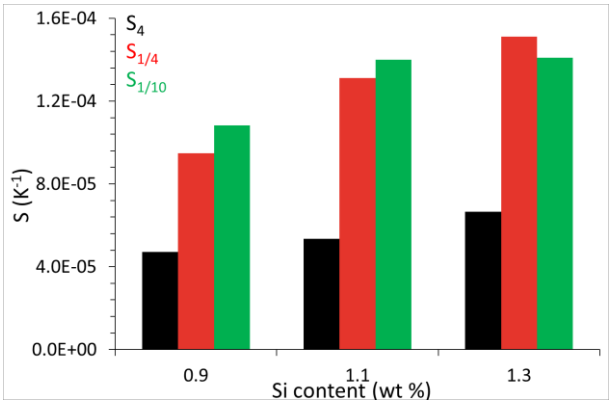

Figure 7: *A summary of S_4 (black), $S_{1/4}$ (red), and $S_{1/10}$ (green), taken from the Haasen plots in Fig. 6, using the analysis methods described for Fig. 5a-c.*

The results show that an addition of Si increases S_4 and $S_{1/4}$, as well as the difference between S_4 and $S_{1/4}$.

5.0 Discussion

In order to investigate the role of clusters formed during natural ageing, as detected by DSC, on the up-change and down-change strain rate sensitivity, one can plot the evolution of the apparent activation volume normalized by b^3 with strain hardening. Figures 8a-c shows the data points and fitting to the constant thermodynamic strain rate sensitivity, S, obtained from the Haasen slope.

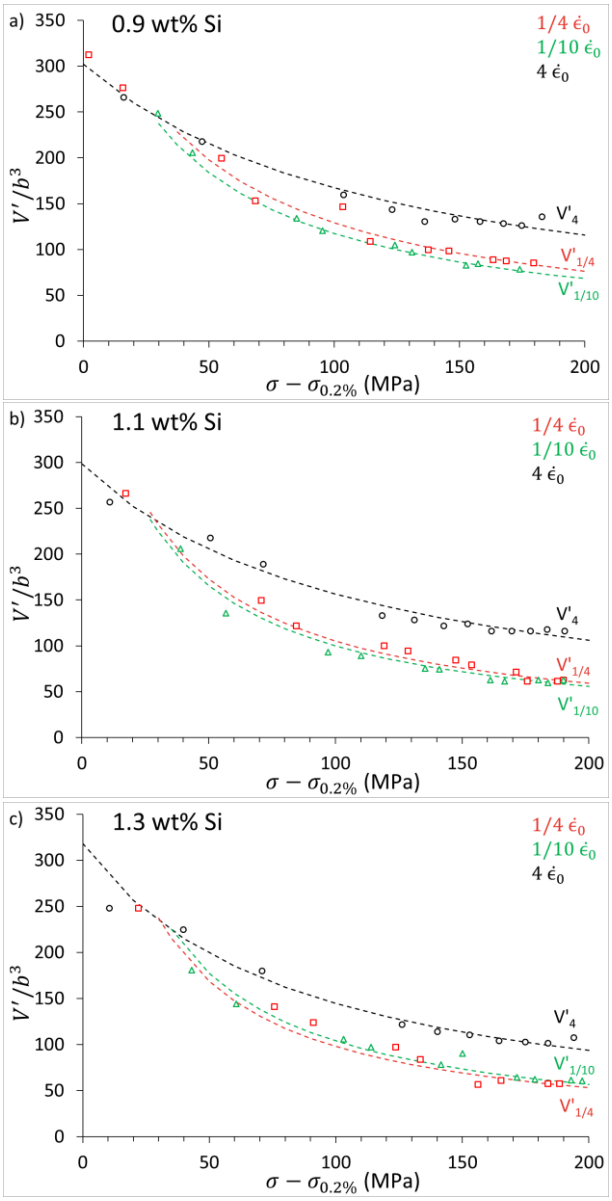

Figure 8: *The evolution of the normalized apparent activation volume versus reduced stress for the up-changes (open black circles), 1/4 (open red squares) and 1/10 (open green triangles), each with the corresponding modeled curves based on the respective SRS shown in the coloured dashed line for the* ***a)*** *0.9 wt% Si,* ***b)*** *1.1 wt% Si, and* ***c)*** *1.3 wt% Si alloys.*

For all alloys tested, the apparent activation volume after initial yielding is similar at around 300 b^3. With straining, the apparent activation volume progressively decreases, as is expected from the increasing dislocation density that follows V'_4 or the S_4 lines in Figures 5a-c. The activation volume measured by down-change tests ($V'_{1/4}$ and $V'_{1/10}$) starts to decrease more than the up-change measurements after some deformation incubation suggesting that a different or second mechanism/obstacle is present. One explanation for this bifurcation could be dissolution of the solute clusters into smaller more complex objects, as described by Chen et al. [50] for Al-Cu, which ultimately decreases the apparent activation volume via a decrease in both the activation distance, d, and spacing of the obstacles, l, such that V' = bdl decreases. An alternative mechanism for the decrease could be dislocation interactions in the solute cluster field during straining generating dislocation debris (small loops), which are weak obstacles that recover rapidly during the down-changes, though this effect is unexpected at such low strains [51], [52]

Based on the calculated S values shown for the three alloys in Figure 7, it is possible to estimate the activation distance, representative of the size of the rate-controlling obstacles, based on the relationship:

$$(\sigma - \sigma_{0.2\%})V' = Mk/S \qquad (6)$$

Assuming that the Taylor equation applies, $(\sigma - \sigma_{0.2\%}) = M\alpha\mu b/l$, where α represents the obstacle strength associated with forest dislocations (0.3 used in this work), μ, the temperature dependent shear modulus of aluminium (24 739 MPa at 294 K) and l represents the obstacle spacing along the dislocation line, then

$$(\sigma - \sigma_{0.2\%})V' = \left(\frac{M\alpha\mu b}{l}\right)(bdl)$$
$$= M\alpha\mu b^2 d = Mk/S \qquad (7)$$

The activation distance d, can be calculated from the Haasen plot, and normalized by the Burgers vector, as represented in Figure 9 for the three alloys from the up and down strain rate changes as well as the difference.

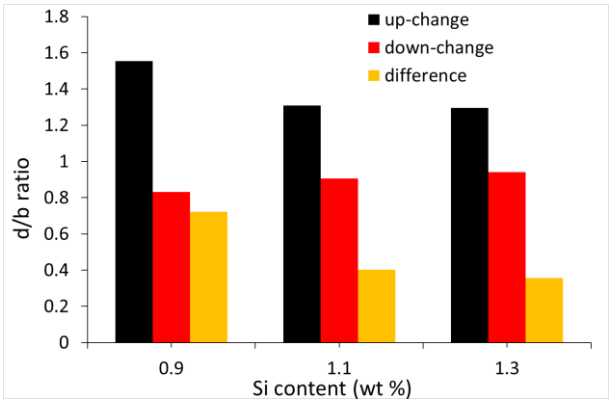

Figure 9: *The evolution of the d/b ratio for the up-change (black) and down-change (red) tests, with the difference (yellow) for each alloy tested in this work. The down-change values were taken from both the 1/4 and 1/10 tests in combination determined, the slopes of* $V'vs.(\sigma - \sigma_{0.2\%})^{-1}$ *plots were taken from after the separation between the up- and down-change difference to eliminate effects of cluster contribution.*

These results show that addition of Si slightly increases the down-change apparent obstacle size while having the contrary effect on the up-change values. The decrease in the up-change obstacle size follows the same trends found by Niewczas et al. [21] whereby additions of Mg was found to decrease d/b for up-change tests in Al-Mg alloys. It can be pointed out that the Niewczas et al. measurements were performed at 78 K compared to 294 K in the present case, with the latter temperature having much increased solute mobility and dislocation recovery, hence the significantly larger d/b ratio in the present work.

The increase in the down-change obstacle size with Si content contrasts with what Niewczas et al. [21] found at 78K with Mg, whereby Mg additions also decreased the d/b ratio. The likely cause of this is the ability for dislocation-dislocation and dislocation-solute/cluster interaction products to be recovered during the down-change strain rate change [53] whereby there is an effect on the spacing l, rather than d. Niewczas and Park [53] showed that in pure Al, dislocation-dislocation interaction products do not anneal out at temperatures below 100K; in contrast, such recoverable components must be considered here. Saimoto [29] and Saimoto and Duesbery [51] have argued that the presence of these dislocation interaction products contribute to the SRS in the down-change at ambient temperatures due to their likelihood to anneal out during the rate-change; in the strain rate change test, this effect would appear as an added relaxation during a perfectly compensated strain rate change. This would be coupled with the extensive work performed by Niewczas [52], [53] for observing the dislocation interaction products at low temperatures and the corresponding annealing temperatures, and how they influence the flow stress. It could be argued that certain dislocation-dislocation or dislocation-solute interaction products are able to influence the apparent obstacles size, being a second type of obstacle present and detectable during the strain rate change tests. A larger d/b indicates the presence of thermally activable obstacles that are stronger in nature and thus, the relative increase in d/b with increased Si content may suggest that the production of these complex products depends on the Si content of the alloy whereby increased Si promotes the formation of dislocation-dislocation interaction products.

The evolution of the d/b ratio for the up-change and down-change tests have clearly shown a distinct asymmetry that is directly related to the SRS difference. If it is proposed that the difference in the SRS between the down-change and up-change tests are due to the evolution or recovery of another type of obstacle, the difference in stress-change will be termed the asymmetric stress contributions (ASC), $\Delta\sigma_{ASC}$, related to the asymmetric SRS by

$$S_{ASC} = S_{dc} - S_{uc} \tag{8}$$

where S_{ASC} is the SRS of the asymmetric stress contributions (see Figure 10), and S_{dc} and S_{uc} are the down-change and up-change SRS values at high flow stresses (those after the deviation between up-change and down-change tests), respectively. From the calculation of S_{ASC}, the relative change in the flow stress due to the strain rate change test may be calculated by using Eq. 4 but substituting in the new S_{ASC}

$$\Delta\sigma_{ASC} = S_{ASC}(\sigma - \sigma_{0.2\%})T\Delta \ln \dot{\epsilon}_{ucdc} \tag{9}$$

where $\Delta \ln \dot{\epsilon}_{ucdc}$ is the difference in strain rate between the up-change and down-change strain rates. It is interesting that the evolution of the ASC may be calculated and plotted versus strain hardening for the total ASC as shown in Figure 10.

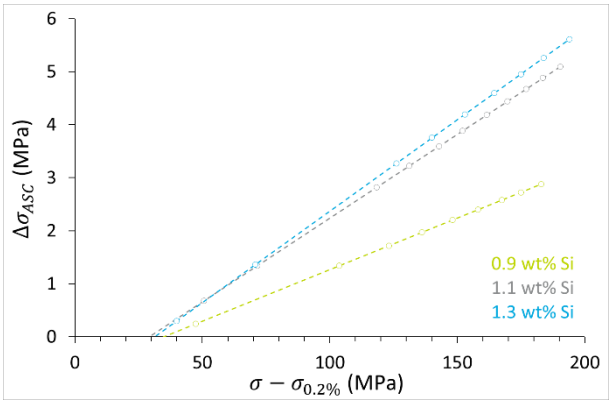

Figure 10: *The evolution of the asymmetric stress contribution for the varying levels of Si. The production rate of the asymmetric stress contribution appears to increase with Si content while the onset of the deviation appears to be independent of Si content. Note that the $S_{1/4}$ values were used along with the S_4 to produce this plot.*

Figure 10 clearly shows an evolution in the rate of ASC accumulation with increased Si content while the onset of the ASC does not appear to be affected. If the premise of recoverable dislocation products and recovery is postulated to be responsible for the evolution of the ASC, it may be said that the addition of Si either increases the amount of recoverable debris being produced or Si increases the ability of the produced debris to be recovered. Both of these postulations would result in a net increase in the slope of Figure 10.

The implications of the asymmetry in the SRS are connected directly to the deformation beyond uniform elongation during a tensile test. The differences in the up- and down-change SRS will separately affect the interior and exterior parts of the diffuse neck, respectively, that develops during plastic deformation as the local strain rate is no longer equal to the imposed rate resulting in changes to the local stress states. Additionally, we have shown that higher Si results in increased uniform elongation while simultaneously increasing both the up- and down-change SRS suggesting that alloys with higher Si contents may be more favourable for forming operations.

6.0 Conclusions

- The use of compensation during down-change strain rate jump tests enables more precise measurement of stress changes due to strain rate changes by taking into account the change in machine stiffness.
- The strain rate sensitivity in the studied 6000-series aluminium alloys was observed at 294K to depend both on the magnitude of the strain rate change and on its sign. A difference between up- and down-changes was observed after an incubation strain hardening of 40 MPa (equivalent to about 0.04 plastic strain). At larger strains the down-change thermodynamic strain rate sensitivity, S, becomes substantially larger than that of up-change tests and the magnitude of the stress changes becomes dependent on the magnitude of the rate change.
- The apparent activation distance derived from the up-change tests decreases with Si content indicating that the rate-controlling obstacles are more strongly thermally activated; the opposite correlation was found for Si additions and down-change tests.
- In the considerations of formability and the transition between diffuse and local necking, due to the large difference between increasing or decreasing rate changes, it may be important to consider how the SRS affects the local stress state within the neck interior and exterior.

7.0 Acknowledgements

The authors would like to thank the Association Nationale Recherche Technologie (ANRT) for co-funding the project.

8.0 Data Availability

The raw/processed data required to reproduce these findings cannot be shared at this time due to legal or ethical reasons.

9.0 References

[1] J. Hirsch, 'Automotive trends in aluminium-The European perspective', in *Materials Forum*, 2004, vol. 28, pp. 15–23.

[2] J. Hirsch, 'Recent development in aluminium for automotive applications', *Trans. Nonferrous Met. Soc. China*, vol. 24, no. 7, pp.

1995–2002, Jul. 2014, doi: 10.1016/S1003-6326(14)63305-7.
[3] M. Considère, *Mémoire sur l'emploi du fer et de l'acier dans les constructions*, vol. 1. Dunod, 1885.
[4] A. K. Ghosh, 'The Influence of Strain Hardening and Strain-Rate Sensitivity on Sheet Metal Forming', *J. Eng. Mater. Technol.*, vol. 99, no. 3, p. 264, 1977, doi: 10.1115/1.3443530.
[5] K. W. Neale and E. Chater, 'Limit strain predictions for strain-rate sensitive anisotropic sheets', *Int. J. Mech. Sci.*, vol. 22, no. 9, pp. 563–574, Jan. 1980, doi: 10.1016/0020-7403(80)90018-1.
[6] A. K. Ghosh, 'Tensile instability and necking in materials with strain hardening and strain-rate hardening', *Acta Metall.*, vol. 25, no. 12, pp. 1413–1424, Dec. 1977, doi: 10.1016/0001-6160(77)90072-4.
[7] B. J. Diak and S. Saimoto, 'Role of Strain Rate Sensitivity on Diffuse Necking', in *Dynamic Plasticity and Structural Behaviours*, 1995, pp. 5–8.
[8] J. W. Hutchinson and K. W. Neale, 'SHEET NECKING-III. STRAIN-RATE EFFECTS', p. 17.
[9] J. W. Hutchinson and K. W. Neale, 'Influence of strain-rate sensitivity on necking under uniaxial tension', *Acta Metall.*, vol. 25, no. 8, pp. 839–846, Aug. 1977, doi: 10.1016/0001-6160(77)90168-7.
[10] E. W. Hart, 'Theory of the tensile test', *Acta Metall.*, vol. 15, no. 2, pp. 351–355, Feb. 1967, doi: 10.1016/0001-6160(67)90211-8.
[11] Y. M. Wang and E. Ma, 'Strain hardening, strain rate sensitivity, and ductility of nanostructured metals', *Mater. Sci. Eng. A*, vol. 375–377, pp. 46–52, Jul. 2004, doi: 10.1016/j.msea.2003.10.214.
[12] N. Chibane, H. Ait-Amokhtar, and C. Fressengeas, 'On the strain rate dependence of the critical strain for plastic instabilities in Al-Mg alloys', *Scr. Mater.*, vol. 130, pp. 252–255, Mar. 2017, doi: 10.1016/j.scriptamat.2016.11.037.
[13] S. Esmaeili, L. M. Cheng, A. Deschamps, D. J. Lloyd, and W. J. Poole, 'The deformation behaviour of AA6111 as a function of temperature and precipitation state', *Mater. Sci. Eng. A*, vol. 319–321, pp. 461–465, Dec. 2001, doi: 10.1016/S0921-5093(01)01113-3.
[14] B. J. Diak, K. R. Upadhyaya, and S. Saimoto, 'Characterization of thermodynamic response by materials testing', *Prog. Mater. Sci.*, vol. 43, no. 4, pp. 223–363, 1998.
[15] W. A. Curtin, 'New interpretation of the Haasen plot for solute-strengthened alloys', *Scr. Mater.*, vol. 63, no. 9, pp. 917–920, Nov. 2010, doi: 10.1016/j.scriptamat.2010.07.003.
[16] P. S. BATE, 'The effects of combined strain-path and strain-rate changes in aluminum', *Metall. Trans. A*, p. 11.
[17] R. C. Picu, F. Ozturk, E. Esener, and R. Li, 'Aluminum Alloys with Identical Plastic Flow and Different Strain Rate Sensitivity', *Metall. Mater. Trans. A*, vol. 41, no. 13, pp. 3358–3364, Dec. 2010, doi: 10.1007/s11661-010-0423-z.
[18] M. Carlone and S. Saimoto, 'Precision strain rate sensitivity measurement using the step-ramp method', *Exp. Mech.*, vol. 36, no. 4, pp. 360–366, 1996.
[19] S. Gupta, A. J. Beaudoin, and J. Chevy, 'Strain rate jump induced negative strain rate sensitivity (NSRS) in aluminum alloy 2024: Experiments and constitutive modeling', *Mater. Sci. Eng. A*, vol. 683, pp. 143–152, Jan. 2017, doi: 10.1016/j.msea.2016.12.010.
[20] B. J. Diak, *Microplastic bases for constitutive characterization of aluminum alloys and their correlation to sheet formability*. 1997.
[21] M. Niewczas, M. Jobba, and R. K. Mishra, 'Thermally activated flow of dislocations in Al–Mg binary alloys', *Acta Mater.*, vol. 83, pp. 372–382, Jan. 2015, doi: 10.1016/j.actamat.2014.09.056.
[22] L. Ding, Z. Jia, Z. Zhang, R. E. Sanders, Q. Liu, and G. Yang, 'The natural aging and precipitation hardening behaviour of Al-Mg-Si-Cu alloys with different Mg/Si ratios and Cu additions', *Mater. Sci. Eng. A*, vol. 627, pp. 119–126, Mar. 2015, doi: 10.1016/j.msea.2014.12.086.
[23] M. Murayama, K. Hono, W. F. Miao, and D. E. Laughlin, 'The effect of Cu additions on the precipitation kinetics in an Al-Mg-Si alloy with excess Si', *Metall. Mater. Trans. A*, vol. 32, no. 2, pp. 239–246, 2001.
[24] Y. Weng, Z. Jia, L. Ding, Y. Pan, Y. Liu, and Q. Liu, 'Effect of Ag and Cu additions on natural aging and precipitation hardening behavior in Al-Mg-Si alloys', *J. Alloys Compd.*, vol. 695, pp.

2444–2452, Feb. 2017, doi: 10.1016/j.jallcom.2016.11.140.
[25] M. W. Zandbergen, A. Cerezo, and G. D. W. Smith, 'Study of precipitation in Al–Mg–Si Alloys by atom probe tomography II. Influence of Cu additions', *Acta Mater.*, vol. 101, pp. 149–158, Dec. 2015, doi: 10.1016/j.actamat.2015.08.018.
[26] M. R. Langille *et al.*, 'Understanding the Role of Cu and Clustering on Strain Hardening and Strain Rate Sensitivity of Al-Mg-Si-Cu Alloys', in *Light Metals 2019*, 2019, pp. 143–151.
[27] F. R. N. Nabarro, 'Cottrell-Stokes law and activation theory', *Acta Metall. Mater.*, vol. 38, no. 2, pp. 161–164, 1990.
[28] R. C. Picu and R. Li, 'On the relationship between the Cottrell–Stokes law and the Haasen plot', *Mater. Sci. Eng. A*, vol. 527, no. 20, pp. 5303–5306, Jul. 2010, doi: 10.1016/j.msea.2010.04.093.
[29] S. Saimoto, 'Dynamic dislocation–defect analysis', *Philos. Mag.*, vol. 86, no. 27, pp. 4213–4233, Sep. 2006, doi: 10.1080/14786430500367347.
[30] A. H. Cottrell and R. J. Stokes, 'Effects of Temperature on the Plastic Properties of Aluminium Crystals', *Proc. R. Soc. Math. Phys. Eng. Sci.*, vol. 233, no. 1192, pp. 17–34, Dec. 1955, doi: 10.1098/rspa.1955.0243.
[31] S. Saimoto and H. Sang, 'A re-examination of the cottrell-stokes relation based on precision measurements of the activation volume', *Acta Metall.*, vol. 31, no. 11, pp. 1873–1881, Nov. 1983, doi: 10.1016/0001-6160(83)90133-5.
[32] S. Saimoto, J. Cooley, H. Larsen, and C. Scholler, 'Kinetic analysis of dynamic point defect pinning in aluminium initiated by strain rate changes', *Philos. Mag.*, vol. 89, no. 10, pp. 853–868, Apr. 2009, doi: 10.1080/14786430902791730.
[33] J. R. Klepaczko and C. Y. Chiem, 'On rate sensitivity of f.c.c. metals, instantaneous rate sensitivity and rate sensitivity of strain hardening', *J. Mech. Phys. Solids*, vol. 34, no. 1, pp. 29–54, Jan. 1986, doi: 10.1016/0022-5096(86)90004-9.
[34] P. Haasen, 'Plastic deformation of nickel single crystals at low temperatures', *Philos. Mag.*, vol. 3, no. 28, pp. 384–418, Apr. 1958, doi: 10.1080/14786435808236826.
[35] M. J. Starink and S. C. Wang, 'A model for the yield strength of overaged Al–Zn–Mg–Cu alloys', *Acta Mater.*, vol. 51, no. 17, pp. 5131–5150, 2003.
[36] E. Hornbogen and E. A. Starke Jr, 'Overview no. 102 Theory assisted design of high strength low alloy aluminum', *Acta Metall. Mater.*, vol. 41, no. 1, pp. 1–16, 1993.
[37] L. C. Wong and S. Saimoto, 'Superposition of thermal activation processes in quenched aluminum-1.7 at% copper', *Scr. Metall. Mater.*, vol. 29, no. 3, pp. 341–346, 1993.
[38] X. Wang, S. Esmaeili, and D. J. Lloyd, 'The sequence of precipitation in the Al-Mg-Si-Cu alloy AA6111', *Metall. Mater. Trans. A*, vol. 37, no. 9, pp. 2691–2699, 2006.
[39] S. Esmaeili and D. J. Lloyd, 'Characterization of the evolution of the volume fraction of precipitates in aged AlMgSiCu alloys using DSC technique', *Mater. Charact.*, vol. 55, no. 4–5, pp. 307–319, Nov. 2005, doi: 10.1016/j.matchar.2005.07.007.
[40] V. Fallah, B. Langelier, N. Ofori-Opoku, B. Raeisinia, N. Provatas, and S. Esmaeili, 'Cluster evolution mechanisms during aging in Al–Mg–Si alloys', *Acta Mater.*, vol. 103, pp. 290–300, Jan. 2016, doi: 10.1016/j.actamat.2015.09.027.
[41] V. Fallah *et al.*, 'Atomic-scale pathway of early-stage precipitation in Al–Mg–Si alloys', *Acta Mater.*, vol. 82, pp. 457–467, Jan. 2015, doi: 10.1016/j.actamat.2014.09.004.
[42] Y. Aruga, M. Kozuka, Y. Takaki, and T. Sato, 'Effects of natural aging after pre-aging on clustering and bake-hardening behavior in an Al–Mg–Si alloy', *Scr. Mater.*, vol. 116, pp. 82–86, Apr. 2016, doi: 10.1016/j.scriptamat.2016.01.019.
[43] J. Kim, E. Kobayashi, and T. Sato, 'Effects of Cu addition on behavior of nanoclusters during multi-step aging in Al-Mg-Si alloys', *Mater. Trans.*, vol. 52, no. 5, pp. 906–913, 2011.
[44] S. Kim, J. Kim, H. Tezuka, E. Kobayashi, and T. Sato, 'Formation behavior of nanoclusters in Al–Mg–Si alloys with different Mg and Si concentration', *Mater. Trans.*, vol. 54, no. 3, pp. 297–303, 2013.
[45] G. H. Tao, C. H. Liu, J. H. Chen, Y. X. Lai, P. P. Ma, and L. M. Liu, 'The influence of Mg/Si ratio on the negative natural aging effect in Al–Mg–Si–Cu alloys', *Mater. Sci. Eng. A*, vol.

642, pp. 241–248, Aug. 2015, doi: 10.1016/j.msea.2015.06.090.
[46] L. Cao, P. A. Rometsch, and M. J. Couper, ‘Effect of pre-ageing and natural ageing on the paint bake response of alloy AA6181A’, *Mater. Sci. Eng. A*, vol. 571, pp. 77–82, Jun. 2013, doi: 10.1016/j.msea.2013.01.065.
[47] D. Yin *et al.*, ‘Effect of natural ageing and pre-straining on the hardening behaviour and microstructural response during artificial ageing of an Al–Mg–Si–Cu alloy’, *Mater. Des.*, vol. 95, pp. 329–339, Apr. 2016, doi: 10.1016/j.matdes.2016.01.119.
[48] C. P. Ling and P. G. McCormick, ‘The effect of temperature on strain rate sensitivity in an Al-Mg-Si alloy’, *Acta Metall. Mater.*, vol. 41, no. 11, pp. 3127–3131, 1993.
[49] C. P. Ling and P. G. McCormick, ‘Strain rate sensitivity and transient behaviour in an Al Mg Si alloy’, *Acta Metall. Mater.*, vol. 38, no. 12, pp. 2631–2635, 1990.
[50] Y. Chen, M. Weyland, and C. R. Hutchinson, ‘The effect of interrupted aging on the yield strength and uniform elongation of precipitation-hardened Al alloys’, *Acta Mater.*, vol. 61, no. 15, pp. 5877–5894, Sep. 2013, doi: 10.1016/j.actamat.2013.06.036.
[51] S. Saimoto and M. S. Duesbery, ‘Strain rate sensitivity: the role of dislocation loop and point defect recovery’, *Acta Metall.*, vol. 32, no. 1, pp. 147–155, 1984.
[52] M. Niewczas, ‘Transmission electron microscopy observations of debris structure in deformed copper single crystals’, *Philos. Mag. A*, vol. 82, no. 2, pp. 393–414, Jan. 2002, doi: 10.1080/01418610208239607.
[53] M. Niewczas and D.-Y. Park, ‘Flow stress and electrical resistivity in plastically deformed Al subjected to intermittent annealing’, *Mater. Sci. Eng. A*, vol. 706, pp. 256–268, 2017.